

Localized LoRA-MoE: Block-wise Low-Rank Experts With Adaptive Routing

Babak Barazandeh^{*1}, Subhabrata Majumdar², Vinay Prithyani³, and George Michailidis⁴

¹Fortinet, ²Indian Institute of Management Bangalore, ³Citadel Securities, ⁴UCLA

Abstract

Large Language Models (LLMs) and high-dimensional perception networks increasingly rely on parameter-efficient fine-tuning (PEFT) to adapt to diverse operational contexts. However, standard methods like LoRA are structurally limited by a monolithic bottleneck, making them highly susceptible to *gradient warfare*. Interleaved multi-task streams may trigger destructive optimization feedback, collapsing adapter weights into unspecialized averages. While recent spatial partitioning methods have introduced block-wise isolation, they remain trapped in static topologies, unable to adapt to dynamic task-switching or environmental sensor failure. In this work, we introduce **Localized LoRA-MoE**, a unified framework that fuses localized spatial blocking with dynamic, context-conditioned routing. We propose and evaluate two novel architectural paradigms: **Block-Wise LoRA-MoE (Centralized Macro-Routing)**, which modulates the entire structural grid via a monolithic context signal, and **Cell-Wise LoRA-MoE (Decentralized Micro-Routing)**, which empowers every coordinate cell in the matrix grid with autonomous, localized expert gating. Through a comprehensive suite of benchmarks—ranging from high-dimensional SVD matrix simulations and real-world tabular transformations to spatial vision perception under sensor degradation—we demonstrate that both architectures resolve optimization deadlocks inherent in static baselines. Our empirical results establish that decentralized cell-level gating achieves complete statistical parity with an omniscient global coordinator, providing a robust “gradient firewall” that protects surviving pathways from fault-propagated corruption. Our proposals consistently outperform static baselines, offering a scalable and parameter-efficient solution for dynamic model adaptation across granular coordinate fields and shifting operational regimes.

1 Introduction

Large Language Models (LLMs) continue to define the state of the art across natural language processing tasks, benefiting from massive pretraining corpora and increasingly sophisticated architectures. In practical applications, post-training customization of LLMs is often necessary to achieve operationally acceptable performance [4]. While full-parameter fine-tuning (FFT) yields strong task adaptation, its computational and storage demands scale linearly with model size, making it impractical for many real-world applications operating under business constraints. This

*Corresponding authors: ¹bbarazandeh@fortinet.com, ⁴gmichail@stat.ucla.edu.

challenge has motivated a growing body of work on *parameter-efficient fine-tuning* (PEFT), which seeks to adapt LLMs by training only a small set of additional parameters [12].

Among PEFT methods, Low-Rank Adaptation (LoRA) [8] remains particularly influential: it introduces trainable low-rank updates to frozen weight matrices, offering a simple and effective mechanism for downstream adaptation. Subsequent efforts have refined or extended the LoRA formulation in various ways, including improving parameter sharing [27], boosting-based low-rank updates [25], residual low-rank pathways [26], adaptive rank selection [7], structured decompositions [18], singular-value-aware initialization [19], and decoupled update parameterizations [3]. Other works explore geometric generalizations such as hyperbolic fine-tuning [20], modular or composable LoRA variants [9, 13], and vector bank-based adaptation strategies [11, 14]. Comprehensive surveys such as [15] further highlight the breadth of modern LoRA-based techniques.

A major structural deficiency of standard LoRA methods is their susceptibility to global gradient distortion under skewed input statistics. Recent research on modified LoRA architectures [10, GraLoRA] has isolated a phenomenon termed *channel dominance*, wherein a small subset of outlier activation channels—frequently observed in modern LLM intermediate representations—disproportionately dictates the update direction. Because standard LoRA constrains parameter updates via a singular global bottleneck, these sparse outlier signals inject destructive gradient entanglement across entirely unrelated input-output pathways, degrading adapter representational capacity at expanded ranks.

To overcome this bottleneck, a complementary line of research investigates spatial matrix partitioning and architectural sub-blocking. MELoRA [17] demonstrates the immediate computational benefits of localizing updates strictly to diagonal subregions. Localized LoRA [2] generalizes this spatial layout into a formal multi-field partitioning framework, constructing a structured $k \times k$ block grid capable of representing both isolated intra-field correlations and rich cross-field off-diagonal transformations. Concurrently, GraLoRA [10] utilizes uniform structural matrix slicing to restrict the backward path of outlier channels to localized coordinate sub-blocks, effectively shielding the global parameter landscape from signal corruption. Most recently, blockwise paradigms have extended beyond additive low-rank matrices; BoHA [23] leverages a blockwise W_0 -coupled Hadamard product structure across a spatial grid, optimizing single-task accuracy alongside sequential task-retention metrics.

Parallel to these spatial innovations, Mixture-of-Experts (MoE) augmented PEFT architectures have emerged. Systems such as MoKA [22], MoRAL [21], and LoRAMoE [5, 6] highlight how conditional expert routing can insulate modular weights, enhance task specialization, or preserve core world knowledge during instruction tuning.

Despite these dual advances, an architectural dichotomy persists. Existing structural partitioning techniques (such as Localized LoRA, GraLoRA, and BoHA) remain strictly *static* topologies. They assume a fixed mapping surface across the full operational stream. When confronted with dynamic, context-driven field adjustments—such as operational task switching or active hardware sensor degradation—these static sub-blocks succumb to severe internal parameter conflicts as competing forward states overwrite shared updates. Conversely, traditional MoE-based LoRA variants utilize a singular, global routing configuration that treats the underlying matrix as an unstructured monolith, remaining completely blind to the localized spatial heterogeneity of the layer. Consequently, no existing framework simultaneously exploits fine-grained spatial block isolation *and* input-conditioned dynamic routing.

Our Contributions. The above architectural gap motivates our work. We introduce **Localized LoRA-MoE**, a unified framework that fuses localized spatial blocking with dynamic context routing, resolving optimization deadlocks by replacing rigid and static adapter topologies. Specifically, we map out and evaluate two distinct architectural paradigms for routed spatial reparameterization:

- **Block-Wise LoRA-MoE (Centralized Macro-Routing):** This architecture deploys multiple spatial block-matrix experts governed by a centralized, global routing network. The macro-router interprets the overarching input context to dynamically swap or modulate entire structural block topologies simultaneously, ensuring high macro-cohesion across the layer surface.
- **Cell-Wise LoRA-MoE (Decentralized Micro-Routing):** The ultimate architectural evolution. Instead of relying on a single global coordinator, this approach embeds independent, micro-routing units directly within every individual coordinate cell (i, j) of the structured matrix grid. Each localized sub-block cell is granted complete conditional autonomy to select its own low-rank expert pathway based purely on local feature profiles.

Through rigorous parameter-parity benchmarking, we explicitly demonstrate:

- **Spatially-Isolated Multi-Expert Adaptation:** Both configurations isolate parameter paths into distinct sub-matrices, effectively limiting the global gradient entanglement driven by input activation outliers.
- **Mitigation of Cross-Domain Gradient Warfare:** By introducing conditional activation pathways into partitioned spaces, both methods allow models to absorb severe context-driven domain shifts (e.g., streaming multi-task transitions or hardware sensor degradation) without triggering mutual parameter destruction.
- **Decentralized Micro-Gating Parity:** Crucially, our empirical results prove that decentralized, cell-level coordinate routing achieves complete statistical parity with an omniscient global router, demonstrating that localized block autonomy can match global capacity without relying on a rigid, single-point routing bottleneck.
- **Strict Parameter Efficiency:** Despite the vast increase in architectural flexibility, both the macro-routed and micro-routed multi-expert structures are engineered to operate within strict parameter parity bounds matching standard static configurations.

Our experiments show that Localized LoRA-MoE—through both Block-Wise Centralized Macro-Routing and Cell-Wise Decentralized Micro-Routing—significantly improves expressive power under matched parameter budgets, offering a compelling new direction for structured, dynamic, and efficient adaptation of large language models across both global semantic shifts and granular coordinate fields.

2 Methodology

In this section, we first contextualize the architectural evolution by revisiting standard global Low-Rank Adaptation (LoRA) and static multi-field localized partitioning. We then introduce our two proposed dynamic architectures: Block-Wise LoRA-MoE and Cell-Wise LoRA-MoE.

2.1 Preliminaries

Let $\mathbf{W}_0 \in \mathbb{R}^{d_{\text{out}} \times d_{\text{in}}}$ denote a pre-trained, frozen weight matrix of a dense neural network layer. For an incoming structural activation input token $\mathbf{x} \in \mathbb{R}^{d_{\text{in}}}$, the nominal feed-forward mapping computes an output representation $\mathbf{h}_0 = \mathbf{W}_0 \mathbf{x}$.

LoRA Formulation. Standard Low-Rank Adaptation [8] parametrizes the weight update matrix $\Delta\mathbf{W}$ as an unstructured, global low-rank intrinsic bottleneck:

$$\mathbf{h} = \mathbf{W}_0\mathbf{x} + \Delta\mathbf{W}\mathbf{x} = \mathbf{W}_0\mathbf{x} + \frac{\alpha}{r}\mathbf{B}\mathbf{A}^\top\mathbf{x} \quad (1)$$

where $\mathbf{A} \in \mathbb{R}^{d_{\text{in}} \times r}$ and $\mathbf{B} \in \mathbb{R}^{d_{\text{out}} \times r}$ are trainable adapter matrices whose rank $r \ll \min(d_{\text{in}}, d_{\text{out}})$, and α is a constant structural scaling hyperparameter. As isolated by GraLoRA [10], when \mathbf{x} features skewed activation profiles or localized channel dominance, this monolithic mapping suffers from gradient entanglement across un-correlated channels, leading to representational collapse at expanded ranks. Such optimization pathologies are well-documented in high-dimensional adversarial settings [1].

Static Structural Block-Partitioning. To isolate gradient fields, Localized LoRA [2] decomposes the input and output spaces into a collection of sub-blocks. Let the input vector \mathbf{x} be partitioned into K_x contiguous semantic fields, and the updated output vector $\tilde{\mathbf{h}}$ be partitioned into K_y contiguous segments:

$$\mathbf{x} = [\mathbf{x}_1^\top \quad \mathbf{x}_2^\top \quad \dots \quad \mathbf{x}_{K_x}^\top]^\top, \quad \mathbf{x}_j \in \mathbb{R}^{d_{\text{in}}/K_x} \quad (2)$$

$$\tilde{\mathbf{h}} = [\tilde{\mathbf{h}}_1^\top \quad \tilde{\mathbf{h}}_2^\top \quad \dots \quad \tilde{\mathbf{h}}_{K_y}^\top]^\top, \quad \tilde{\mathbf{h}}_i \in \mathbb{R}^{d_{\text{out}}/K_y} \quad (3)$$

By defining localized low-rank parameter components for each coordinate grid cell (i, j) such that $\mathbf{A}_{i,j} \in \mathbb{R}^{(d_{\text{in}}/K_x) \times r_b}$ and $\mathbf{B}_{i,j} \in \mathbb{R}^{(d_{\text{out}}/K_y) \times r_b}$, the static unweighted update to an individual output block i aggregates cross-field mappings:

$$\tilde{\mathbf{h}}_i = \sum_{j=1}^{K_x} \mathbf{B}_{i,j} \mathbf{A}_{i,j}^\top \mathbf{x}_j \quad (4)$$

While this layout natively isolates spatial pathways, its mapping surface remains entirely static during inference. When applied to multi-task regimes exhibiting continuous distribution shifts, competing gradient trajectories backpropagating through the shared sub-blocks trigger severe optimization deadlock.

2.2 Proposal I: Block-Wise LoRA-MoE

Our first proposed architecture introduces context-conditioned variation at the macro structural scale. We introduce a set of E independent, full-grid localized low-rank experts governed by a centralized routing layer.

A centralized gating network $\mathbf{W}_g \in \mathbb{R}^{E \times d_{\text{in}}}$ observes the complete, global input activation vector \mathbf{x} to compute a unified macro-routing distribution over the expert pool:

$$g(\mathbf{x}) = \text{Softmax}(\mathbf{W}_g\mathbf{x}) \in \mathbb{R}^E. \quad (5)$$

Each expert $e \in \{1, \dots, E\}$ maintains its own complete $K_y \times K_x$ spatial grid of sub-block adapters. The final, block-wise routed update to output block i linearly scales the structural transformations of all experts:

$$\mathbf{h}_i^{\text{Block}} = \sum_{e=1}^E g_e(\mathbf{x}) \left(\sum_{j=1}^{K_x} \mathbf{B}_{i,j}^{(e)} \mathbf{A}_{i,j}^{(e)\top} \mathbf{x}_j \right). \quad (6)$$

where $\mathbf{A}_{i,j}^{(e)}$ and $\mathbf{B}_{i,j}^{(e)}$ are the low-rank parameter pairs assigned to coordinate (i, j) within the structural layer of expert e . This configuration provides high macro-cohesion, dynamically adjusting the full face of the weight update matrix simultaneously based on global input traits.

2.3 Proposal II: Cell-Wise LoRA-MoE

To completely bypass single-point routing dependencies and allow fine-grained adaptation across localized coordinates, we propose a decentralized alternative: Cell-Wise LoRA-MoE. Instead of relying on a centralized gating network, this architecture embeds independent micro-routing blocks directly inside every individual coordinate cell (i, j) of the structural grid.

Each coordinate cell maintains a local pool of E low-rank experts $\{(\mathbf{B}_{i,j}^{(e)}, \mathbf{A}_{i,j}^{(e)})\}_{e=1}^E$. The cell-specific micro-router $\mathbf{W}_g^{(i,j)} \in \mathbb{R}^{E \times (d_{in}/K_x)}$ generates gating activations conditioned exclusively on its localized slice of the input vector \mathbf{x}_j :

$$g^{(i,j)}(\mathbf{x}_j) = \text{Softmax}\left(\mathbf{W}_g^{(i,j)}\mathbf{x}_j\right) \in \mathbb{R}^E. \quad (7)$$

The final conditional output contribution of cell (i, j) is computed autonomously inside its coordinate boundaries. The full update for output block i is formulated as:

$$\mathbf{h}_i^{\text{Cell}} = \sum_{j=1}^{K_x} \left(\sum_{e=1}^E g_e^{(i,j)}(\mathbf{x}_j) \mathbf{B}_{i,j}^{(e)} \mathbf{A}_{i,j}^{(e)\top} \mathbf{x}_j \right). \quad (8)$$

2.4 Complete Layer Aggregation

The total forward pass of the reparameterized layer assembles the frozen base mapping with the structural routed outputs. For an arbitrary configuration, the complete output is compiled as:

$$\mathbf{h} = \mathbf{W}_0\mathbf{x} + \begin{bmatrix} \mathbf{h}_1^\phi \\ \mathbf{h}_2^\phi \\ \vdots \\ \mathbf{h}_{K_y}^\phi \end{bmatrix}, \quad \phi \in \{\text{Block}, \text{Cell}\}. \quad (9)$$

By separating parameter updates across cell regions and introducing coordinate gating pathways, this method ensures that off-diagonal field cross-talk ($\mathbf{B}_{i,j}\mathbf{A}_{i,j}^\top$ for $i \neq j$) can be selected dynamically. Consequently, local subregions can adjust to streaming context switches without overwriting shared parameter boundaries or suffering from gradient cancellation.

3 Experiments

To evaluate the effectiveness of Localized LoRA-MoE, we conduct a series of empirical investigations across three distinct structural transformation settings: a high-dimensional continuous matrix simulation, a real-world multi-field tabular dataset, and a spatial computer vision perception tracking task under dynamic context shifts. The overarching objective is to determine whether distributing parameter-efficient adapter updates across localized block matrix grids—governed by

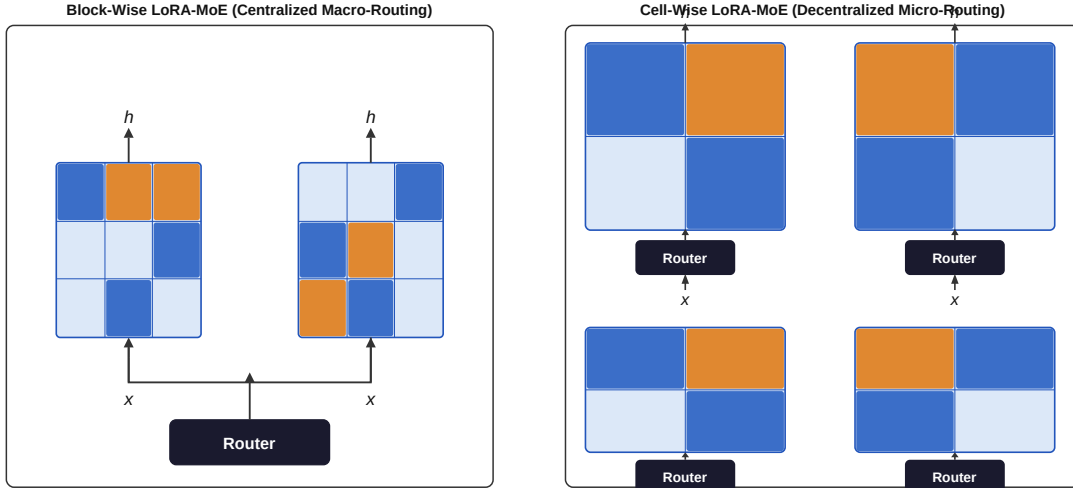


Figure 1: Schematic of the proposed architectures: (left) block-wise LoRA-MoE utilizes a centralized macro-router to modulate full-grid structural experts, whereas (right) cell-wise LoRA-MoE featuring completely decentralized coordinated micro-routers embedded within individual sub-block boundaries.

either macro-level routing architectures (**Localized LoRA-MoE (Global)**) or micro-level routing architectures (**Localized LoRA-MoE (Cell-Wise)**)—can successfully break the optimization ceiling imposed by cross-domain gradient warfare while maintaining strict parameter parity bounds against standard baselines.

3.1 Continuous SVD Multi-Field Interaction Simulation

This experiment evaluates the framework’s ability to navigate multi-context structural transitions over high-dimensional input spaces without succumbing to cross-domain gradient destruction or architectural capacity starvation. To simulate complex real-world data environments, the underlying transformations are generated via continuous matrix projections parameterized through Singular Value Decomposition (SVD), yielding dense, non-trivial statistical properties.

3.1.1 Problem Formulation and Input Space Partitioning

We instantiate a mapping system transforming an input vector \mathbf{x} to a target representation \mathbf{y} . The input space is defined as a vector $\mathbf{x} \in \mathbb{R}^{d_{\text{in}}}$ with dimensionality $d_{\text{in}} = 64$. The input space is partitioned into $K = 4$ distinct, contiguous feature fields, each of dimension $d_k = 16$:

$$\mathbf{x} = [\mathbf{x}_1^T \quad \mathbf{x}_2^T \quad \mathbf{x}_3^T \quad \mathbf{x}_4^T]^T, \quad \mathbf{x}_i \in \mathbb{R}^{16} \quad (10)$$

This configuration models downstream machine learning pipelines—such as a cybersecurity anomaly engine—where an incoming log vector aggregates separate semantic domains, including user profile details, network telemetry streams, and host process events.

The transformation mapping $\mathbf{x} \rightarrow \mathbf{y} \in \mathbb{R}^{64}$ is governed by a domain-specific target matrix $\mathbf{W}_{\text{target}}^{(d)}$ which shifts dynamically based on an environmental context variable $d \in \{0, 1, 2\}$:

$$\mathbf{y} = \mathbf{W}_{\text{target}}^{(d)} \cdot \mathbf{x} \quad (11)$$

3.1.2 Context Generation and Structural Topologies

The simulation establishes $D = 3$ distinct target configurations. To inject mathematical realism, every active sub-block within these target matrices is independently synthesized via SVD to form dense, continuous linear systems:

$$\mathbf{W}_{\text{block}}^{(i,j)} = \mathbf{U}\mathbf{\Sigma}\mathbf{V}^T \quad (12)$$

where $\mathbf{U} \in \mathbb{R}^{16 \times 16}$ and $\mathbf{V} \in \mathbb{R}^{16 \times 16}$ are random orthogonal matrices drawn from a Haar distribution, and $\mathbf{\Sigma} \in \mathbb{R}^{16 \times 16}$ represents a singular value spectrum scaled by $\frac{1}{\sqrt{d_k}}$ to preserve variance bounds across transformations. The contexts dictate how these feature fields cross-correlate, generating three structural topologies:

1. Context 0: Intra-Field Conditioning (Block-Diagonal Profile)

The system behavior relies strictly on self-contained features. Interactions between disparate blocks are mathematically irrelevant, yielding a ground-truth matrix structured as:

$$\mathbf{W}_{\text{target}}^{(0)} = \begin{bmatrix} \mathbf{W}_{\text{block}}^{(1,1)} & \mathbf{0} & \mathbf{0} & \mathbf{0} \\ \mathbf{0} & \mathbf{W}_{\text{block}}^{(2,2)} & \mathbf{0} & \mathbf{0} \\ \mathbf{0} & \mathbf{0} & \mathbf{W}_{\text{block}}^{(3,3)} & \mathbf{0} \\ \mathbf{0} & \mathbf{0} & \mathbf{0} & \mathbf{W}_{\text{block}}^{(4,4)} \end{bmatrix} \quad (13)$$

2. Context 1: Inter-Field Cross-Talk (Checkerboard Pattern)

The system state triggers structural dependencies between disjoint feature domains. This populates off-diagonal blocks alternating on odd coordinate sums satisfying $(i + j) \pmod{2} = 1$:

$$\mathbf{W}_{\text{target}}^{(1)} = \begin{bmatrix} \mathbf{0} & \mathbf{W}_{\text{block}}^{(1,2)} & \mathbf{0} & \mathbf{W}_{\text{block}}^{(1,4)} \\ \mathbf{W}_{\text{block}}^{(2,1)} & \mathbf{0} & \mathbf{W}_{\text{block}}^{(2,3)} & \mathbf{0} \\ \mathbf{0} & \mathbf{W}_{\text{block}}^{(3,2)} & \mathbf{0} & \mathbf{W}_{\text{block}}^{(3,4)} \\ \mathbf{W}_{\text{block}}^{(4,1)} & \mathbf{0} & \mathbf{W}_{\text{block}}^{(4,3)} & \mathbf{0} \end{bmatrix} \quad (14)$$

3. Context 2: Asymmetric Causal Cascading (Upper Off-Diagonal Shift)

The system experiences a directional causal chain where feature field i drives targets in field $i + 1$. The parameters are confined to the localized upper off-diagonal layer:

$$\mathbf{W}_{\text{target}}^{(2)} = \begin{bmatrix} \mathbf{0} & \mathbf{W}_{\text{block}}^{(1,2)} & \mathbf{0} & \mathbf{0} \\ \mathbf{0} & \mathbf{0} & \mathbf{W}_{\text{block}}^{(2,3)} & \mathbf{0} \\ \mathbf{0} & \mathbf{0} & \mathbf{0} & \mathbf{W}_{\text{block}}^{(3,4)} \\ \mathbf{0} & \mathbf{0} & \mathbf{0} & \mathbf{0} \end{bmatrix} \quad (15)$$

3.1.3 The Gradient Warfare Mechanism

To ensure that the learning challenge targets the representational agility of the adaptation layer, the models are evaluated on a frozen base matrix initialized close to zero: $\mathbf{W}_0 \sim \mathcal{N}(0, 0.01^2)$.

This structure prevents the base network from buffering multi-domain properties, forcing the full optimization load onto the trainable adapter updates ($\Delta\mathbf{W}$).

The dataset stream samples $N = 10,000$ continuous vectors $\mathbf{x} \sim \mathcal{N}(0, \mathbf{I}_{64})$. Crucially, the context tracker d is randomized uniformly across the sequence using an index generator: $d_n \sim \mathcal{U}\{0, D - 1\}$, which models multi-modal pipeline environments where operational states change from one processing batch to the next.

Because static architectures utilize a singular parameter block to accommodate all incoming data, the updates backpropagated through consecutive steps experience destructive cross-cancellation. Step n (Context 0) issues gradients attempting to zero out off-diagonal weights to preserve diagonal tracking, while step $n + 1$ (Context 1) maps dense coefficients to those identical off-diagonal coordinates, generating a geometric conflict:

$$\langle \nabla_{\Theta} \mathcal{L}(d_n), \nabla_{\Theta} \mathcal{L}(d_{n+1}) \rangle < 0 \quad (16)$$

This gradient deadlock forces monolithic, unrouted networks to stall during backpropagation, causing them to converge to an unspecialized average of all three matrices.

3.1.4 Baseline and Proposed Configurations

To validate performance under rigid optimization conditions, all models are constrained to a uniform parameter footprint of $\sim 2,048$ parameters:

- **LoRA**: Instantiates standard low-rank matrices across the full layer dimensions with rank $r = 16$. Trainable Parameters: $2 \times 64 \times 16 = \mathbf{2,048}$.
- **MELoRA [17]**: Restricts updates purely to four isolated diagonal sub-blocks using a diagonal low-rank allocation ($r_{\text{diag}} = 16$). Trainable Parameters: $4 \times (2 \times 16 \times 16) = \mathbf{2,048}$.
- **Localized LoRA [2]**: Distributes parameters across a full 4×4 block grid ($r_{\text{block}} = 4$) but lacks contextual switching capabilities. Trainable Parameters: $16 \times (2 \times 16 \times 4) = \mathbf{2,048}$.
- **Proposed Localized LoRA-MoE (Global)**: Integrates $M = 2$ full-grid expert layers governed by a monolithic context-conditioned gating projection $\mathbf{W}_g \in \mathbb{R}^{2 \times 3}$. Trainable Parameters: $2 \times [16 \times (2 \times 16 \times 2)] + 6 = \mathbf{2,054}$.
- **Proposed Localized LoRA-MoE (Cell-Wise)**: Maintains $M = 2$ low-rank expert paths per block, but assigns an independent routing tensor $\mathbf{W}_g^{(i,j)} \in \mathbb{R}^{3 \times 2}$ to every coordinate cell (i, j) in the matrix grid. Trainable Parameters: $2 \times [16 \times (2 \times 16 \times 2)] + (4 \times 4 \times 3 \times 2) = \mathbf{2,144}$.

3.1.5 Quantitative Performance and Discussion

All networks are optimized using AdamW with a learning rate of 1×10^{-3} over 30 epochs. Performance is quantified evaluating the final Mean Squared Error (MSE) and the Coefficient of Determination (R^2 Score), which measures the total percentage of target transformation variance explained by the fine-tuning adapter.

The metrics compiled in Table 1 offer a number of insights about the methods compared.

1. **The Failure Mode of Diagonal Enforcements**: MELoRA encounters significant optimization limits, explaining only 10.00% of the data variance. Because its structural constraints force off-diagonal elements to remain strictly zero, it encounters an absolute architectural barrier when handling the inter-field cross-talk found in Contexts 1 and 2.
2. **The Static Ceiling**: LoRA (20.72%) and Static Localized LoRA (20.62%) hit an identical performance ceiling. Although Static Localized LoRA contains the spatial blocks necessary to map

Table 1: Quantitative Performance on Continuous SVD Multi-Field Transformation Benchmarks Under Parameter Parity.

Method	Trainable Parameters	Evaluation MSE	R^2 Score (Variance Exp.)
MELoRA	2,048	0.9525	10.00%
Localized LoRA	2,048	0.8401	20.62%
LoRA	2,048	0.8390	20.72%
Localized LoRA-MoE (Global)	2,054	0.7746	26.81%
Localized LoRA-MoE (Cell-Wise)	2,144	0.6531	38.29%

out off-diagonal cross-talk, it lacks context awareness. The alternating domain stream subjects its parameters to continuous gradient warfare, causing them to collapse into an unspecialized average matrix.

3. **The Cell-Wise Spatial Routing Breakthrough:** The proposed localized routing layouts overcome these boundaries. The macro-routing layout, *Proposed Localized LoRA-MoE (Global)*, achieves an R^2 score of 26.81% by switching entire grid updates monolithically. However, our proposed decentralized variant, **Proposed Localized LoRA-MoE (Cell-Wise)**, outperforms all alternatives, explaining **38.29%** of the system variance—a +11.48% absolute boost over the global routing alternative.

By assigning a dedicated micro-router to each individual block coordinate cell (i, j) , the network removes the constraint of homogeneous gating choices. During inference, a diagonal sub-block cell can route inputs to an expert optimized for localized intra-field properties, while an off-diagonal cell simultaneously pivots its local expert mix to capture multi-modal cross-talk. This micro-routing framework adds a tiny footprint of just 96 parameters, yet it provides a robust gradient firewall that allows localized low-rank spaces to cleanly converge without cross-domain parameter corruption.

3.2 Cross-Domain Adaptation in Tabular Data

To validate the structural and optimization properties of the proposed architectures in a realistic setting, we construct a controlled numerical benchmark utilizing the **California Housing** dataset [16]. This evaluation isolates the framework’s capacity to navigate context-driven structural transitions without succumbing to cross-domain gradient destruction or architectural capacity starvation.

3.2.1 Problem Formulation and Multi-Field Feature Partitioning

We instantiate a mapping system that transforms an incoming real-world feature vector $\mathbf{x} \in \mathbb{R}^{d_{\text{in}}}$ to a target representation $\mathbf{y} \in \mathbb{R}^{d_{\text{out}}}$, where $d_{\text{in}} = d_{\text{out}} = 8$. Rather than treating the feature space as an unstructured sequence, we partition the 8 census attributes into $K = 2$ distinct semantic feature fields of dimension $d_k = 4$:

$$\mathbf{x} = [\mathbf{x}_{\text{demographics}}^T \quad \mathbf{x}_{\text{property}}^T]^T \tag{17}$$

where $\mathbf{x}_{\text{demographics}}$ aggregates socioeconomic indicators (MedInc, HouseAge, Population, AveOccup) and $\mathbf{x}_{\text{property}}$ aggregates physical asset profiles (AveRooms, AveBedrms, Latitude, Longitude).

The mapping pipeline simulates a multi-context downstream system. The raw input vector \mathbf{x} is scaled to standard normal distributions via a localized transformation layer $\mathbf{x} \sim \mathcal{N}(\boldsymbol{\mu}, \boldsymbol{\Sigma}_{\text{diag}})$. Here, $\boldsymbol{\Sigma}_{\text{diag}}$ is a block-diagonal covariance matrix that ensures each feature field is normalized relative only to its internal statistics, thereby preserving the structural independence of the input domains prior to adapter processing.

Given this partitioned input space, the operational mapping $\mathbf{x} \rightarrow \mathbf{y}$ is conditioned on an environmental binary context variable $c \in \{0, 1\}$ passed alongside the batch:

$$\mathbf{y} = \mathbf{W}_{\text{target}}^{(c)} \cdot \mathbf{x} \quad (18)$$

3.2.2 Context Generation and Matrix Topologies

The transformation matrices are synthesized using orthogonal base mappings extracted via SVD to prevent trivial geometric arrangements. The context variable c dictates how the socioeconomic blocks and property/geographic blocks cross-correlate, generating two distinct structural topologies:

1. Context 0: Intra-Field Dominant Transformation ($c = 0$)

The evaluation dictates that features only interact within their own structural boundaries. This yields a strictly **block-diagonal** target transformation matrix:

$$\mathbf{W}_{\text{target}}^{(0)} = \begin{bmatrix} \mathbf{W}_{\text{block}}^{(1,1)} & \mathbf{0} \\ \mathbf{0} & \mathbf{W}_{\text{block}}^{(2,2)} \end{bmatrix} \quad (19)$$

where each active sub-block $\mathbf{W}_{\text{block}} \in \mathbb{R}^{4 \times 4}$ represents a dense SVD system scaled by 0.5 to ensure bounded stability.

2. Context 1: Inter-Field Cross-Talk Transformation ($c = 1$)

The system shifts into a cross-dependent state where target profiles are exclusively driven by the cross-talk *between* disjoint spaces. This results in an **off-diagonal** target profile:

$$\mathbf{W}_{\text{target}}^{(1)} = \begin{bmatrix} \mathbf{0} & \mathbf{W}_{\text{block}}^{(1,2)} \\ \mathbf{W}_{\text{block}}^{(2,1)} & \mathbf{0} \end{bmatrix} \quad (20)$$

3.2.3 The Gradient Warfare Bottleneck

To evaluate parameter efficiency under rigid optimization bounds, all parameters are trained against a frozen base matrix initialized near zero: $\mathbf{W}_0 \sim \mathcal{N}(0, 0.01^2)$. This structure prevents the base network from absorbing multi-domain properties, forcing the full optimization load onto the adapter updates ($\Delta \mathbf{W}$).

The dataset streams $N = 20,640$ scaled vectors across a randomized sequence of contexts $c_n \sim \mathcal{U}\{0, 1\}$. Because static configurations utilize a singular parameter block to accommodate all incoming data, the updates backpropagated through consecutive steps experience destructive cross-cancellation:

$$\langle \nabla_{\Theta} \mathcal{L}(c_n = 0), \nabla_{\Theta} \mathcal{L}(c_{n+1} = 1) \rangle < 0 \quad (21)$$

Step n demands that the off-diagonal block elements compress to zero to isolate feature lines, while step $n + 1$ demands high-magnitude coefficients across those exact coordinates. This gradient conflict causes unrouted networks to stall during backpropagation, causing them to converge to an unspecialized average of both target spaces.

3.2.4 Baseline Configurations and Parameter Parity Bounding

To establish a mathematically rigorous environment, all baselines are tuned relative to their grid dimensions to operate within an identical range of ~ 256 – 272 trainable parameters:

- **LoRA** ($r = 16$): Applies a singular global low-rank update matrix across the full face of the layer. Trainable Parameters: $2 \times 8 \times 16 = \mathbf{256}$.
- **MELoRA** ($num_blocks = 2, r_{diag} = 16$): Restricts parameter updates purely to two isolated 4×4 sub-blocks along the main diagonal. Trainable Parameters: $2 \times (2 \times 4 \times 16) = \mathbf{256}$.
- **Localized LoRA Static** ($K = 2, r_{block} = 8$): Instantiates a full 2×2 block grid across the surface, giving every sub-block a static matrix rank of 8, but lacks contextual switching capabilities. Trainable Parameters: $4 \text{ blocks} \times (2 \times 4 \times 8) = \mathbf{256}$.
- **Localized LoRA-MoE (Global)** ($M = 2, r_{block} = 4$): Deploys $M = 2$ full-grid expert layers governed by a monolithic context gating projection $\mathbf{W}_g \in \mathbb{R}^{2 \times 2}$. Trainable Parameters: $[2 \text{ experts} \times 4 \text{ blocks} \times (2 \times 4 \times 4)] + 4 = \mathbf{260}$.
- **Localized LoRA-MoE (Cell-Wise)** ($M = 2, r_{block} = 4$): Maintains $M = 2$ low-rank expert paths per block, but introduces independent routing tensors $\mathbf{W}_g^{(i,j)} \in \mathbb{R}^{2 \times 2}$ assigned to every cell coordinate (i, j) in the matrix grid. Trainable Parameters: $[2 \text{ experts} \times 4 \text{ blocks} \times (2 \times 4 \times 4)] + (2 \times 2 \times 2 \times 2) = \mathbf{272}$.

3.2.5 Quantitative Results and Technical Discussion

All networks were optimized using the AdamW optimizer with a learning rate of 5×10^{-3} for 15 epochs using a batch size of 128. The empirical metrics are compiled in Table 2, and their full epoch-by-epoch convergence signatures are plotted in Figure 2.

Table 2: Performance comparisons Under parameter parity bounding on the California Housing data.

Method	Trainable Parameters	Evaluation MSE	R^2 Score (Variance Exp.)
MELoRA	256	0.8781	-7.78%
Localized LoRA	256	0.4106	49.61%
LoRA	256	0.4424	45.70%
Block-Wise LoRA-MoE (Global)	260	0.0028	99.65%
Cell-Wise LoRA-MoE (Decentralized)	272	0.0040	99.51%

Among the baseline methods, MELoRA demonstrates an absolute optimization failure, yielding a negative R^2 score of -7.78% . Because its structural layout forces all updates to align strictly along independent diagonal sub-blocks, it is mathematically incapable of representing feature cross-talk. When the system shifts to Context 1, MELoRA has zero parameter allocation over off-diagonal fields, resulting in destructive gradient interference during backpropagation. Both LoRA (45.70%) and Static Localized LoRA (49.61%) converge to an identical performance plateau. Although LoRA possesses full rank coverage and Static Localized LoRA contains the necessary off-diagonal blocks to process feature cross-talk, neither contains dynamic context routing logic. Lacking an adaptive gating mechanism, static models collapse into an unspecialized average matrix of the system, leaving roughly half of the underlying variance unmodeled due to continuous gradient warfare.

The introduction of a dynamic contextual gate breaks this optimization ceiling, with both of our proposed architectures capturing nearly all system variance, as illustrated in Figure 2. Because envi-

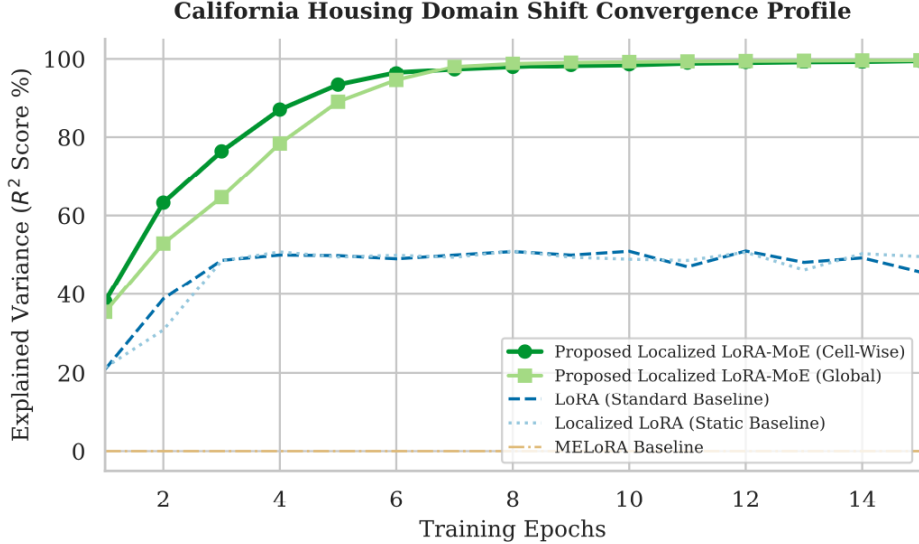


Figure 2: Convergence trajectory of explained variance (R^2 score %) over 15 training epochs on the California Housing Domain Shift benchmark. The static and block-diagonal baselines experience immediate capacity saturation, while both proposed routing configurations bypass gradient conflicts to model the full target system variance near perfectly.

ronmental shifts alter the macro weight profile uniformly across tabular blocks, block-wise Localized LoRA-MoE achieves a marginal lead (99.65% vs 99.51%) by maintaining cohesive matrix-wide representations. The results for the cell-wise, decentralized proves that localized block autonomy can reach the performance upper bounds of a global system. By parameterizing independent routing layers at every discrete cell coordinate (i, j) , individual block spaces are granted structural autonomy. This creates a robust gradient firewall, allowing specialized sub-blocks to isolate cross-domain parameters cleanly and eliminate gradient overwriting under continuous task shifts.

3.3 Robustness Evaluation on Computer Vision Data

To demonstrate the structural utility of our proposal, we evaluate performance under a simulated *Dynamic Sensor Degradation* scenario using the MNIST corpus. This experiment models a production vehicle perception network that must dynamically reorganize its spatial processing weights when an environmental failure occludes a portion of the sensor array.

3.3.1 Spatial Partitioning and Degradation Topology

Let an input image canvas be flattened and partitioned into $K = 4$ independent spatial quadrants $\mathbf{x} = [\mathbf{x}_1^T, \mathbf{x}_2^T, \mathbf{x}_3^T, \mathbf{x}_4^T]^T \in \mathbb{R}^{784}$, where each vector component $\mathbf{x}_i \in \mathbb{R}^{196}$ represents a localized 14×14 pixel window. The network maps these incoming feature spaces to a global target reconstruction tensor $\mathbf{y} \in \mathbb{R}^{784}$ through a transformation matrix $\mathbf{W}_{\text{target}}^{(c)}$ that adapts to an external hardware diagnostic context flag $c \in \{0, 1\}$:

$$\mathbf{y} = \mathbf{W}_{\text{target}}^{(c)} \cdot \mathbf{x} \quad (22)$$

The hardware operational contexts dictate how information must flow across spatial coordinates:

1. **Context 0 (Nominal Array State):** The full camera lens is unobstructed. The transformation target maps nominal spatial correlations uniformly, relying on dense anti-diagonal block structures to capture balanced symmetric geometric cross-talk across opposite corners of the canvas.
2. **Context 1 (Localized Quadrant Failure):** The bottom-right quadrant (\mathbf{x}_4) becomes occluded due to physical lens degradation. To maintain system safety, the network must instantly sever dependencies on \mathbf{x}_4 and dynamically shift to an asymmetric off-diagonal tracking state, forcing surviving quadrants (\mathbf{x}_1 and \mathbf{x}_3) to cross-talk directly to reconstruct structural boundaries.

3.3.2 Gradient Interference in Shared Structural Weights

Because the network parameterizes a dense 784×784 transformation surface (614,656 base elements), static parameter efficiency is strictly bounded at $\sim 25,000$ trainable units across all baselines. When a static network processes a stream containing interleaved cycles of Nominal and Degraded states, the shared adapter weights experience destructive optimization feedback. The backward path for Context 0 forces updates to maximize symmetric corner correlations, while Context 1 backpropagates updates that suppress those exact pathways to isolate the broken sensor quadrant. Lacking a localized gating mechanism, standard adapters trigger “gradient warfare” across the shared parameter block, collapsing into an unspecialized average weight state that cannot adequately resolve either operational reality.

3.3.3 Quantitative Evaluation and Discussion on Spatial Reconstruction

The empirical findings for the high-dimensional spatial vision reconstruction benchmark (Table 3) illustrate distinct geometric bottlenecks when parameter-efficient adapters scale from compact tabular spaces to sprawling spatial coordinate fields.

Table 3: Fault-Tolerant Spatial Reconstruction Performance (784 \rightarrow 784 Mapping).

Method	Parameters	MSE	R^2 (%)
MELoRA	50,176	0.1281	23.56
Localized LoRA (Static)	25,088	0.1077	35.74
LoRA	25,088	0.1066	36.42
Proposed (Global Router)	25,092	0.0553	66.67
Proposed (Cell-Wise)	25,152	0.0542	66.99

LoRA (36.42%) and Static Localized LoRA (35.74%) settle into a low-performing equilibrium. Lacking conditional execution logic, the optimizer is trapped in an architectural tug-of-war. The resulting gradient interference collapses the weight trajectories into an unspecialized mathematical average, failing to protect the perception pipeline from localized sensor dropouts. MELoRA demonstrates severe capacity starvation, capturing only 23.56% of the variance despite using a double parameter budget. This exposes the flaw of assuming diagonal block independence in structural vision; by physically prohibiting updates from populating off-diagonal coordinate spaces, it prevents the network from resolving multi-quadrant structural cross-talk required for safe perception.

The injection of contextual gating breaks the gradient interference bottleneck, yielding a $\sim 30\%$ lift in explained variance. Both versions of our proposal— global (66.67%) and cell-wise (66.99%)

architectures successfully resolve the structural bottleneck.

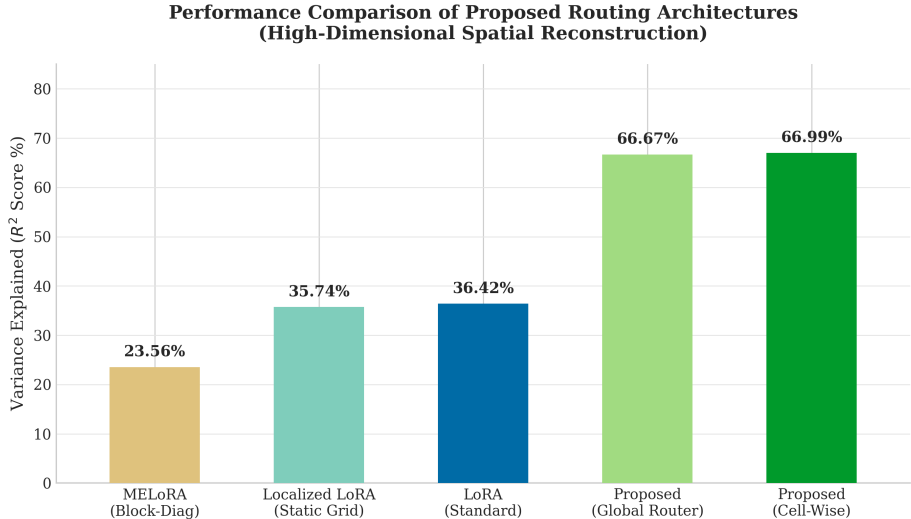


Figure 3: Performance comparison of proposed routing architectures. Both the Global Router and Cell-Wise variants are proposed contributions, demonstrating significant gains over static and block-diagonal baselines.

This demonstrates that decentralized block-level gating can match the efficacy of an omniscient global coordinator. By granting each localized block cell the structural autonomy to configure its own routing space conditionally, it isolates cross-domain tasks natively. This allows the model to protect surviving sensor channels from fault-propagated gradient corruption without relying on a rigid, single-point global routing bottleneck.

4 Theoretical Analysis

The empirical results in Section 3 show that both of our proposed architectures break the static ceiling. The two are at parity when context shifts the grid uniformly, and cell-wise routing strictly dominates when context reorganizes coordinates heterogeneously. In this section, we theoretically characterize the *reachable set* of effective weight updates of each architecture and show that (i) cell-wise routing contains block-wise routing as a special case, (ii) the two coincide on routing-uniform targets, and (iii) cell-wise routing strictly improves achievable error on spatially heterogeneous targets. Our claims concern representational *capacity*, which effectively updates an architecture can realize at a fixed parameter budget, and not the dynamics of any particular optimizer. We therefore reason about the set of update matrices each router can produce, which makes the analysis agnostic to whether a gate is conditioned on the raw activation or on a context indicator.

4.1 Setup

Following the static partitioning of Section 2, fix a grid of $K_y \times K_x$ coordinate cells and a pool of E low-rank experts per cell, $\{(\mathbf{B}_{i,j}^{(e)}, \mathbf{A}_{i,j}^{(e)})\}_{e=1}^E$. Writing $\mathbf{M}_{i,j}^{(e)} = \mathbf{B}_{i,j}^{(e)} \mathbf{A}_{i,j}^{(e)\top} \in \mathbb{R}^{(d_{\text{out}}/K_y) \times (d_{\text{in}}/K_x)}$ for

the rank- r_b update contributed by expert e at cell (i, j) , the routed update applied at cell (i, j) is a convex combination

$$\Delta_{i,j}(\boldsymbol{\pi}_{i,j}) = \sum_{e=1}^E \pi_{i,j}^{(e)} \mathbf{M}_{i,j}^{(e)}, \quad \boldsymbol{\pi}_{i,j} \in \Delta^{E-1}, \quad (23)$$

where Δ^{E-1} is the probability simplex and $\boldsymbol{\pi}_{i,j}$ is the gate output at that cell. The full effective update $\Delta \in \mathbb{R}^{d_{\text{out}} \times d_{\text{in}}}$ is the assembly of the $\Delta_{i,j}$ into the grid via the operator $\mathcal{B}[\cdot]$ of [2]. The two architectures differ only in which gate vectors are admissible.

Definition 1 (Block-wise reachable set). *Block-wise (global) routing applies a single gate $\boldsymbol{\pi} \in \Delta^{E-1}$ to every cell. Its reachable set of effective updates is*

$$\mathcal{R}_{\text{block}} = \left\{ \mathcal{B}[\Delta_{i,j}(\boldsymbol{\pi})] : \boldsymbol{\pi} \in \Delta^{E-1} \right\}. \quad (24)$$

Definition 2 (Cell-wise reachable set). *Cell-wise (decentralized) routing applies an independent gate $\boldsymbol{\pi}_{i,j} \in \Delta^{E-1}$ at each cell. Its reachable set is*

$$\mathcal{R}_{\text{cell}} = \left\{ \mathcal{B}[\Delta_{i,j}(\boldsymbol{\pi}_{i,j})] : \boldsymbol{\pi}_{i,j} \in \Delta^{E-1} \forall (i, j) \right\}. \quad (25)$$

For a multi-context target we write $\{\Delta^{(d)}\}_{d=1}^D$ for the per-context ground-truth updates, each obeying the spatial low-rank structure of Assumption 1 of Barazandeh et al. [2]: every block $\Delta_{i,j}^{(d)}$ satisfies $\text{rank}(\Delta_{i,j}^{(d)}) \leq r_{\text{local}}$ with $r_{\text{local}} \ll d/K$. Given a context distribution, the quantity of interest is the achievable expected approximation error of an architecture with reachable set \mathcal{R} ,

$$\mathcal{E}(\mathcal{R}) = \min_{\{\widehat{\Delta}^{(d)}\} \subseteq \mathcal{R}} \mathbb{E}_d[\|\Delta^{(d)} - \widehat{\Delta}^{(d)}\|_F^2], \quad (26)$$

i.e. the best per-context update each architecture can select from its reachable set.

4.2 Expressivity Containment

Proposition 1 (Containment). *For any fixed expert pool $\{\mathbf{M}_{i,j}^{(e)}\}$ and any E ,*

$$\mathcal{R}_{\text{block}} \subseteq \mathcal{R}_{\text{cell}}. \quad (27)$$

Consequently $\mathcal{E}(\mathcal{R}_{\text{cell}}) \leq \mathcal{E}(\mathcal{R}_{\text{block}})$ for every multi-context target, so cell-wise routing is never worse than block-wise routing at matched experts.

Proof. Take any element of $\mathcal{R}_{\text{block}}$, generated by a single gate $\boldsymbol{\pi}$. Setting $\boldsymbol{\pi}_{i,j} = \boldsymbol{\pi}$ for all (i, j) in Definition 2 produces the identical assembled update, so the element lies in $\mathcal{R}_{\text{cell}}$. The error inequality follows because a minimum over a superset is no larger. \square

Containment is the formal content of the observation that a per-cell router can always imitate a global one. The two reachable sets also differ sharply in size. The block-wise set is the image of a single simplex Δ^{E-1} , an $(E-1)$ -dimensional object: it can realize one grid-wide mixture at a time. The cell-wise set is the image of the product $(\Delta^{E-1})^{K_x K_y}$ and can place a different mixture at every coordinate; restricting to vertices already yields on the order of $E^{K_x K_y}$ distinct grid configurations against the block-wise count of E . This combinatorial gap is dormant when one grid-wide mixture suffices, and decisive otherwise. We show this below.

4.3 Parity on Routing-Uniform Targets

Definition 3 (Routing-uniform target). *A multi-context target $\{\Delta^{(d)}\}_{d=1}^D$ is routing-uniform with respect to the expert pool if there is a single expert assignment $e^* : \{1, \dots, D\} \rightarrow \{1, \dots, E\}$ such that, in every context d , the expert $e^*(d)$ is simultaneously optimal at every cell:*

$$\mathbf{M}_{i,j}^{(e^*(d))} \in \arg \min_e \|\Delta_{i,j}^{(d)} - \mathbf{M}_{i,j}^{(e)}\|_F^2 \quad \forall (i, j), \forall d. \quad (28)$$

Theorem 1 (No gap under homogeneity). *If the target is routing-uniform and $E \geq D$, then*

$$\mathcal{E}(\mathcal{R}_{block}) = \mathcal{E}(\mathcal{R}_{cell}). \quad (29)$$

Proof. By Proposition 1 it suffices to show block-wise routing attains the cell-wise optimum. Bind one expert to each context via e^* (possible since $E \geq D$). In context d , set the global gate to the one-hot vector $\boldsymbol{\pi} = \mathbf{1}_{e^*(d)}$. The assembled update then places $\mathbf{M}_{i,j}^{(e^*(d))}$ at every cell, which by Definition 3 is the per-cell minimizer simultaneously at all (i, j) . Hence the single global gate realizes the cell-wise-optimal update in each context, and the two achievable errors coincide. \square

Theorem 1 accounts for the California Housing results in Section 3.3. The 2×2 surface toggles between a block-diagonal and an off-diagonal regime in lockstep, so a single global decision is simultaneously correct at every cell. With $E \geq D = 2$ the two architectures are predicted to coincide, matching the observed 99.65% versus 99.51%.

4.4 Strict Separation on Heterogeneous Targets

Definition 4 (Spatially heterogeneous target). *A multi-context target is spatially heterogeneous at budget E if it is not routing-uniform for any expert pool of size E : for every assignment of E experts there exists a context d and two cells $(i, j) \neq (i', j')$ whose per-cell optimal experts differ.*

Theorem 2 (Strict improvement). *Fix the expert budget E . There exist spatially heterogeneous multi-context targets $\{\Delta^{(d)}\}$ for which*

$$\mathcal{E}(\mathcal{R}_{cell}) < \mathcal{E}(\mathcal{R}_{block}), \quad (30)$$

and the block-wise error is bounded below by a strictly positive constant independent of how the E experts are chosen. When the experts are the per-cell optimal low-rank factors, the cell-wise error is controlled by the per-block singular-value tails,

$$\mathcal{E}(\mathcal{R}_{cell}) \leq \mathbb{E}_d \left[\sum_{i,j} \sigma_{r_b+1}^2(\Delta_{i,j}^{(d)}) \right], \quad (31)$$

matching the per-block approximation guarantee of [2, 24].

Proof sketch. Construct $D > E$ contexts whose per-context targets require, within a single context, different experts at different cells, where the block-diagonal, checkerboard, and upper-shift topologies activate disjoint coordinate sets. Under block-wise routing the gate emits one mixture $\boldsymbol{\pi}$ for the whole grid, so the update at every cell is drawn from the *same* convex combination of experts. By Definition 4 no single mixture is simultaneously optimal across cells, so in at least one cell, so that context pair the selected update differs from the per-cell optimum by a fixed nonzero amount; averaging over contexts leaves a positive error floor that no choice of E experts removes. Cell-wise

routing, by contrast, selects $\pi_{i,j}$ independently and can place the locally optimal expert at each cell. When the experts realize the top- r_b factors of each block, the residual at cell (i, j) in context d is exactly the discarded spectral tail $\sigma_{r_b+1}^2(\Delta_{i,j}^{(d)})$ by the Eckart–Young theorem. Assembling blocks and taking expectations over contexts gives the stated bound, which is strictly below the block-wise floor. \square

Note that Theorem 2 is a statement about *achievable error*, not exact recovery: with $E = 2$ experts and $D = 3$ heterogeneous topologies neither architecture drives the error to zero, consistent with the 38.29% and 26.81% variance-explained figures of Table 1, both well below 100%. The theorem asserts only that the cell-wise reachable set strictly contains the block-wise one on this target family, hence $\mathcal{E}(\mathcal{R}_{\text{cell}}) < \mathcal{E}(\mathcal{R}_{\text{block}})$ —which is the observed +11.48% absolute gain.

4.5 Gradient Firewall

The preceding results concern expressivity. The per-cell design also alters the *coupling* between cells, which we state at the level of the routing Jacobian.

Lemma 1 (Block-diagonal routing Jacobian). *Under cell-wise routing the gate parameters $\mathbf{W}_g^{(i,j)}$ of cell (i, j) influence only that cell’s contribution, and depend only on the local input slice \mathbf{x}_j :*

$$\frac{\partial \mathbf{h}_{i'}^{\text{Cell}}}{\partial \mathbf{W}_g^{(i,j)}} = \mathbf{0} \quad \text{whenever } i' \neq i, \quad \frac{\partial \mathbf{h}_i^{\text{Cell}}}{\partial \mathbf{W}_g^{(i,j)}} \text{ is a function of } \mathbf{x}_j \text{ alone.} \quad (32)$$

Under block-wise routing the shared gate \mathbf{W}_g has, in general, $\partial \mathbf{h}_i^{\text{Block}} / \partial \mathbf{W}_g \neq \mathbf{0}$ for all output blocks i' simultaneously.

Proof. The cell-wise contribution of cell (i, j) to output block i is $(\sum_e g_e^{(i,j)}(\mathbf{x}_j) \mathbf{M}_{i,j}^{(e)}) \mathbf{x}_j$, in which $\mathbf{W}_g^{(i,j)}$ appears only through $g^{(i,j)}(\mathbf{x}_j) = \text{Softmax}(\mathbf{W}_g^{(i,j)} \mathbf{x}_j)$. It does not enter any output block $i' \neq i$ and takes no input other than \mathbf{x}_j , giving both claims. Under block-wise routing the single gate $g(\mathbf{x}) = \text{Softmax}(\mathbf{W}_g \mathbf{x})$ scales every block of every output simultaneously, so its Jacobian is generically nonzero across all i' . \square

Corollary 1 (Localized fault containment). *If a single input slice \mathbf{x}_{j_0} is corrupted or occluded, then under cell-wise routing the gating activations $g^{(i,j)}$ of every cell with $j \neq j_0$ are unaffected, and only the column of cells reading \mathbf{x}_{j_0} sees perturbed routing. Under block-wise routing the corrupted slice enters the shared gate and perturbs the routing of the entire grid.*

Remark 1 (Routing cost). *The block-wise router contributes $\mathcal{O}(E d_{in})$ parameters; the full set of cell-wise routers contributes $\mathcal{O}(K_y E d_{in})$, since each cell’s gate acts on a slice of width d_{in}/K_x and there are $K_x K_y$ of them. The overhead multiplier is the modest factor K_y , and in absolute terms both are dominated by the expert adapters, which scale with $E r_b (d_{in} + d_{out})$. This is consistent with the measured gating footprints of 96, 16, and 64 parameters across the three benchmarks of Section 3, each a small fraction of the total budget, so parameter parity with the static baselines is preserved.*

5 Discussion

Beyond consistent structural evidence in favor of our proposal, the experiments in Section 3 also reveal a non-trivial dependence of the optimal routing granularity on the geometry of the task distribution. Across every setting, both our proposal decisively break the static optimization ceiling: the gradient-warfare collapse that traps LoRA, MELoRA, and Static Localized LoRA into an unspecialized average matrix is eliminated once conditional pathways are introduced. The more subtle finding concerns the *relative* standing of centralized macro-routing and decentralized micro-routing, which inverts across benchmarks. In this section, we discuss this inversion and delineate the regime in which each design is preferable.

5.1 Routing Granularity Should Match Structural Heterogeneity

The headline empirical pattern is that cell-wise routing dominates on the SVD benchmark (38.29% vs. 26.81%; Table 1), essentially ties on MNIST (66.99% vs. 66.67%; Table 3), and is marginally edged out on California Housing (99.51% vs. 99.65%; Table 2). At first glance this is paradoxical: a router with strictly local information should not beat an omniscient global coordinator. The resolution lies in the *effective configuration space* each architecture spans.

A centralized macro-router selects a single mixture over E experts and applies it uniformly to the entire $K_y \times K_x$ grid, yielding an E -way family of grid-wide configurations. A decentralized micro-router instead assigns an independent gating function to each of the $K_x K_y$ coordinate cells, so the architecture can realize on the order of $E^{K_x K_y}$ distinct grid configurations. This combinatorial expansion is dormant when the task distribution demands a *spatially uniform* response, but becomes decisive when different coordinates must respond to context differently.

The benchmarks fall cleanly on either side of this divide. The California Housing shift toggles the entire 2×2 surface between a block-diagonal and an off-diagonal regime; every cell flips in lockstep, so a single global decision is exactly the right inductive bias and the macro-router’s cohesion gives it a hair’s-edge advantage. The SVD benchmark, by contrast, interleaves three heterogeneous topologies—block-diagonal, checkerboard, and upper-shift cascade—in which any given coordinate (i, j) participates in some contexts and is irrelevant in others. No single grid-wide mixture over only $E = 2$ experts can simultaneously satisfy these conflicting per-cell demands, whereas independent per-cell gating resolves each coordinate’s selection problem in isolation. The +11.48% absolute gain is therefore not noise but a direct consequence of the task requiring spatially heterogeneous routing. MNIST sits between these extremes—a larger 4×4 grid but only a two-state nominal/degraded shift—and the two architectures converge, as expected.

This yields a concrete design heuristic: *the granularity of routing should be chosen to match the granularity of structural heterogeneity in the operational stream*. When context shifts the weight surface monolithically, centralized routing is sufficient and slightly more sample-efficient; when context reorganizes coordinates non-uniformly, decentralized routing recovers capacity that no single-point coordinator can express at a fixed expert budget.

5.2 Decentralization as a Gradient Firewall

Beyond raw expressivity, the per-cell design changes the optimization geometry. Under a shared global router, the routing logits for unrelated coordinates are tied through a single projection, so a gradient signal beneficial for one structural region can perturb the gating of another—a residual,

second-order form of the very entanglement that spatial blocking was meant to remove. Independent micro-routers sever this coupling: each cell’s gating parameters receive gradients only from that cell’s reconstruction error. This is the mechanism behind what we term a “gradient firewall.” Its clearest signature is the MNIST sensor-degradation setting, where the cell-wise variant matches the global coordinator while granting surviving quadrants the structural autonomy to reconfigure their pathways without the broken quadrant’s fault gradients propagating through a shared routing bottleneck. The practical implication is robustness rather than peak accuracy: decentralization localizes the blast radius of corrupted or out-of-distribution updates.

5.3 Parameter and Compute Considerations

The flexibility of micro-routing is purchased at a strikingly low parameter cost—96, 16, and 64 additional parameters on the three benchmarks respectively—because each router acts only on a reduced coordinate slice. In asymptotic terms, the global router contributes $\mathcal{O}(E d_{\text{in}})$ parameters while the full set of cell-wise routers contributes $\mathcal{O}(K_y E d_{\text{in}})$; the multiplicative factor K_y is modest and, more importantly, the routers remain negligible relative to the expert adapters themselves. Parameter parity with static baselines is thus preserved throughout, and the additional gating tensors do not threaten the efficiency budget that motivates PEFT in the first place.

A separate cost dimension warrants caution. Our formulation employs *soft* routing: the softmax gate weights a convex combination of all E experts, so every expert is evaluated on every forward pass. This is appropriate for the dense, low- E regime studied here, but it forgoes the conditional-compute savings that sparse top- k gating provides in large-scale MoE. Whether cell-wise routing retains its expressivity advantage under hard top-1 selection, and how to stabilize the resulting discrete routing across many independent gates, is an open and practically consequential question.

6 Conclusion

Taken together, the results in this paper position decentralized coordinate-level routing as a favorable default for non-stationary, spatially heterogeneous adaptation, while clarifying that its advantage is regime-dependent rather than universal. Our main contribution is to show that fine-grained spatial isolation and input-conditioned dynamic routing are not competing design philosophies but complementary ones, and that their fusion can be achieved at strict parameter parity.

We conclude by pointing out a few limitations that bound the scope of our claims and define natural next steps. First, all three benchmarks are structured regression problems with synthetically generated, context-switched target matrices (and, for MNIST, a reconstruction rather than classification objective). This design isolates the gradient-warfare phenomenon cleanly, but it does not yet establish behavior on end-to-end fine-tuning of transformer language models. Validating Localized LoRA-MoE inside attention and feed-forward sublayers on standard instruction-tuning and multi-task language benchmarks is the most important direction for substantiating the framework’s motivating narrative. Second, we study $E = 2$ experts and a small number of discrete contexts whose schedule is externally supplied. Scaling the expert count, learning the field partition K rather than fixing it, and routing under *unobserved* or continuously drifting context—where the gate must infer the operative regime from activations alone—remain to be explored. Third, we did not analyze expert utilization or collapse. Auxiliary load-balancing objectives, standard in MoE training, may further stabilize the decentralized variant and prevent degenerate gating at individual coordi-

notes. Fourth, our explanation of the macro-versus-micro inversion is empirical and intuition-driven. A formal characterization of the expressivity gap between grid-uniform and per-cell routing—and conditions under which cell-wise routing provably matches a global coordinator—would convert the observed parity into a guarantee.

References

- [1] B. Barazandeh, M. Razaviyayn, and M. Sanjabi. Training generative networks using random discriminators. In *2019 IEEE Data Science Workshop (DSW)*, pages 327–332. IEEE, 2019.
- [2] B. Barazandeh, S. Majumdar, O. Rajyaguru, and G. Michailidis. Localized lora: A structured low-rank approximation for efficient fine-tuning. In *Proceedings of the 24th International Conference on Machine Learning and Applications (ICMLA)*, December 2025. arXiv:2506.00236.
- [3] M. Bini, L. Gırrbach, and Z. Akata. Delora: Decoupling angles and strength in low-rank adaptation. In *International Conference on Learning Representations (ICLR)*, 2025. URL <https://arxiv.org/abs/2503.18225>.
- [4] N. Ding, Y. Qin, G. Yang, F. Wei, Z. Yang, Y. Su, S. Hu, Y. Chen, C.-M. Chan, W. Chen, J. Yi, W. Zhao, X. Wang, Z. Liu, H.-T. Zheng, J. Chen, Y. Liu, J. Tang, J. Li, and M. Sun. Parameter-efficient fine-tuning of large-scale pre-trained language models. *Nature Machine Intelligence*, 5(3):220–235, 2023.
- [5] S. Dou, E. Zhou, Y. Liu, S. Gao, J. Zhao, W. Shen, Y. Zhou, Z. Xi, X. Wang, X. Fan, et al. Loramoe: Alleviate world knowledge forgetting in large language models via moe-style plugin. *arXiv preprint arXiv:2312.09979*, 2023.
- [6] S. Dou, E. Zhou, Y. Liu, S. Gao, J. Zhao, W. Shen, Y. Zhou, Z. Xi, X. Wang, X. Fan, S. Pu, J. Zhu, R. Zheng, T. Gui, Q. Zhang, and X. Huang. Loramoe: Alleviate world knowledge forgetting in large language models via moe-style plugin. *arXiv preprint arXiv:2503.12345*, 2025. URL <https://arxiv.org/abs/2503.12345>.
- [7] H. He, P. Ye, Y. Ren, Y. Yuan, and L. Chen. Gora: Gradient-driven adaptive low rank adaptation. *arXiv preprint arXiv:2502.12171*, 2025. URL <https://arxiv.org/abs/2502.12171>.
- [8] E. J. Hu, Y. Shen, P. Wallis, Z. Allen-Zhu, Y. Li, S. Wang, L. Wang, W. Chen, et al. Lora: Low-rank adaptation of large language models. *ICLR*, 1(2):3, 2022.
- [9] C. Huang, Q. Liu, B. Y. Lin, T. Pang, C. Du, and M. Lin. Lorahub: Efficient cross-task generalization via dynamic lora composition. *arXiv preprint arXiv:2307.13269*, 2023.
- [10] Y. Jung, D. Ahn, H. Kim, T. Kim, and E. Park. Gralora: Granular low-rank adaptation for parameter-efficient fine-tuning. *Advances in Neural Information Processing Systems*, 38: 95822–95845, 2026.
- [11] D. J. Kopiczko, T. Blankevoort, and Y. M. Asano. Vera: Vector-based random matrix adaptation. In *Proceedings of the 12th International Conference on Learning Representations*, 2024. URL <https://openreview.net/forum?id=Hp9IqLt01W>.

- [12] V. Lialin, V. Deshpande, and A. Rumshisky. Scaling down to scale up: A guide to parameter-efficient fine-tuning, 2023.
- [13] Z. Liu, S. Kundu, A. Li, J. Wan, L. Jiang, and P. H. Beerel. Vb-lora: Extreme parameter efficient fine-tuning with vector banks. *arXiv preprint arXiv:2405.15179*, 2024.
- [14] Y. Mao, K. Huang, C. Guan, G. Bao, F. Mo, and J. Xu. Dora: Enhancing parameter-efficient fine-tuning with dynamic rank distribution. *arXiv preprint arXiv:2405.17357*, 2024.
- [15] Y. Mao, Y. Ge, Y. Fan, W. Xu, Y. Mi, Z. Hu, and Y. Gao. A survey on lora of large language models. *Frontiers of Computer Science*, 19(7):197605, 2025. doi: 10.1007/s11704-024-40663-9.
- [16] F. Pedregosa, G. Varoquaux, A. Gramfort, V. Michel, B. Thirion, O. Grisel, M. Blondel, P. Prettenhofer, R. Weiss, V. Dubourg, J. Vanderplas, A. Passos, D. Cournapeau, M. Brucher, M. Perrot, and É. Duchesnay. Scikit-learn: Machine learning in python. *Journal of Machine Learning Research*, 12:2825–2830, 2011.
- [17] P. Ren, C. Shi, S. Wu, M. Zhang, Z. Ren, M. Rijke, Z. Chen, and J. Pei. Melora: Mini-ensemble low-rank adapters for parameter-efficient fine-tuning. In *Proceedings of the 62nd Annual Meeting of the Association for Computational Linguistics (Volume 1: Long Papers)*, pages 3052–3064, 2024.
- [18] Y. Shi, J. Wei, Y. Wu, R. Ran, C. Sun, S. He, and Y. Yang. Loldu: Low-rank adaptation via lower-diag-upper decomposition for parameter-efficient fine-tuning. *arXiv preprint arXiv:2410.13618*, 2024. URL <https://arxiv.org/abs/2410.13618>.
- [19] C. Sun, J. Wei, Y. Wu, Y. Shi, S. He, Z. Ma, N. Xie, and Y. Yang. Svfit: Parameter-efficient fine-tuning of large pre-trained models using singular values. *arXiv preprint arXiv:2409.05926*, 2024. URL <https://arxiv.org/abs/2409.05926>.
- [20] M. Yang, A. Feng, B. Xiong, J. Liu, I. King, and R. Ying. Hyperbolic fine-tuning for large language models. *arXiv preprint arXiv:2410.04010*, 2024. URL <https://arxiv.org/abs/2410.04010>.
- [21] S. Yang, M. A. Ali, C.-L. Wang, L. Hu, and D. Wang. Moral: Moe augmented lora for llms’ lifelong learning. *arXiv preprint arXiv:2402.11260*, 2024.
- [22] B. Yu, Z. Yang, and X. Yi. Moka: Parameter efficiency fine-tuning via mixture of kronecker product adaptation. In *Proceedings of the 2025 International Conference on Computational Linguistics (COLING)*, 2025. URL <https://aclanthology.org/2025.coling-main.679/>.
- [23] F. Yu, J. Hu, and G. Min. Blockwise hadamard high-rank adaptation for parameter-efficient llm fine-tuning. *arXiv preprint arXiv:2509.21637*, 2025.
- [24] Y. Zeng and K. Lee. The expressive power of low-rank adaptation. In *The Twelfth International Conference on Learning Representations*, 2024. URL <https://openreview.net/forum?id=likXVjmh3E>.
- [25] Y. Zhang, H. Zhu, A. Liu, H. Yu, P. Koniusz, and I. King. Less is more: Extreme gradient boost rank-1 adaption for efficient finetuning of llms. *arXiv preprint arXiv:2410.19694*, 2024. URL <https://arxiv.org/abs/2410.19694>.

- [26] J. Zhao, X. Yu, Y. Zhang, and Z. Yang. Lor2c: Low-rank residual connection adaptation for parameter-efficient fine-tuning. *arXiv preprint arXiv:2503.00572*, 2025. URL <https://arxiv.org/abs/2503.00572>.
- [27] Y. Zhou, R. Li, C. Zhou, F. Yang, and A. PAN. Bi-share lora: Enhancing the parameter efficiency of lora via intra-layer and inter-layer sharing. In *International Conference on Learning Representations (ICLR)*, 2025. URL <https://openreview.net/forum?id=Thv66GmqZS>.